AD-A040 165 CALSPAN CORP BUFFALO N Y F/G 17/8
DATA COLLECTION AND MODELING OF IN-FLIGHT INTRINSIC CONTRASTS O--ETC(U)
MAY 77 H B HAMMILL DAAK40-75-C-1114
UNCLASSIFIED CALSPAN-SK-5753-D-1 DRDMI-TD-CR-77-1 NL

| OF |
AD A040165

END

DATE FILMED
6 — 77

TD-CR-77-1

DATA COLLECTION AND MODELING OF IN-FLIGHT INTRINSIC CONTRASTS OF AIRCRAFT

Calspan Corporation
P.O. Box 235
Buffalo, New York 14221

TECHNICAL REPORT TD-CR-77-1
May 1977

US ARMY MISSILE RESEARCH AND DEVELOPMENT COMMAND
(MIRADCOM)
DRDMI-TDW
REDSTONE ARSENAL, ALABAMA 35809

DRDMI-TD

UNCLASSIFIED

SECURITY CLASSIFICATION OF THIS PAGE *(When Data Entered)*

REPORT DOCUMENTATION PAGE	READ INSTRUCTIONS BEFORE COMPLETING FORM
1. REPORT NUMBER: TD-CR-77-1	2. GOVT ACCESSION NO. / 3. RECIPIENT'S CATALOG NUMBER
4. TITLE *(and Subtitle)*: DATA COLLECTION AND MODELING OF IN-FLIGHT INTRINSIC CONTRASTS OF AIRCRAFT	5. TYPE OF REPORT & PERIOD COVERED: Final Report
	6. PERFORMING ORG. REPORT NUMBER: CALSPAN-SK-5753-D-1
7. AUTHOR(s): H. B. Hammill	8. CONTRACT OR GRANT NUMBER(s): DAAK40-75-C-1114
9. PERFORMING ORGANIZATION NAME AND ADDRESS: Calspan Corporation, P.O. Box 235, Buffalo, New York 14221	10. PROGRAM ELEMENT, PROJECT, TASK AREA & WORK UNIT NUMBERS: DA Project Number N/A, AMS Code 2300130865X1
11. CONTROLLING OFFICE NAME AND ADDRESS: US Army Missile Research & Development Command (MIRADCOM) DRDMI-TI, Redstone Arsenal, Alabama 35809	12. REPORT DATE: May 1977
	13. NUMBER OF PAGES: 40 46 P.
14. MONITORING AGENCY NAME & ADDRESS *(if different from Controlling Office)*: US Army Missile Research & Development Command (MIRADCOM) DRDMI-TDW, Redstone Arsenal, Alabama 35809	15. SECURITY CLASS. *(of this report)*: UNCLASSIFIED
	15a. DECLASSIFICATION/DOWNGRADING SCHEDULE

16. DISTRIBUTION STATEMENT *(of this Report)*

Approved for public release; distribution unlimited.

17. DISTRIBUTION STATEMENT *(of the abstract entered in Block 20, if different from Report)*

18. SUPPLEMENTARY NOTES

19. KEY WORDS *(Continue on reverse side if necessary and identify by block number)*

Contrast	Atmosphere Model	Visual Detection
Visual Contrast	Contrast Model	
Aircraft Brightness	Aircraft Reflectance	
Sky Brightness	Optical Models	
Atmospheric Optics		

20. ABSTRACT *(Continue on reverse side if necessary and identify by block number)*

Mathematical modeling to predict the ability of a human observer to visually search and detect aircraft against a sky background requires luminous contrast as an input parameter. This, in turn, depends on average luminance of the aircraft silhouette and its relation to sun angle.

The purpose of the reported study was to test the diffuse (Lambertian) reflecting sphere as a model for introducing illumination geometry,

DD FORM 1 JAN 73 1473 EDITION OF 1 NOV 65 IS OBSOLETE

UNCLASSIFIED

SECURITY CLASSIFICATION OF THIS PAGE *(When Data Entered)*

20. ABSTRACT (Cont.)

principally the solar phase angle, into the prediction of aircraft luminance. The test consisted of a comparison of model prediction with field test data consisting of photographic imagery of a low-altitude aircraft.

The photographic data were reduced through two-dimensional scanning densitometry to yield mean silhouette luminance. These values were compared to values predicted by a diffuse sphere model with the comparison including a full account of atmospherics. A discussion of the comparison is included.

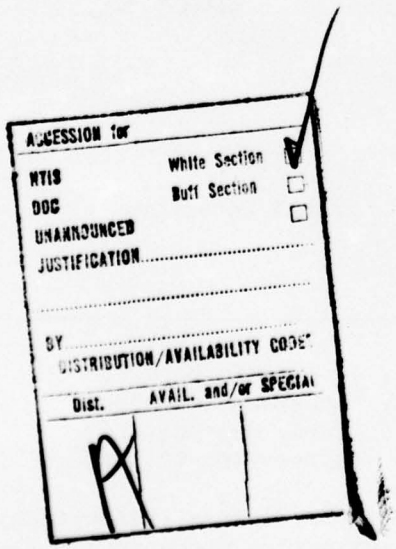

SUMMARY

Visual search for approaching aircraft by ground observers is a part of many system performance evaluations. As a result, several mathematical models exist that quantify the observers' ability, usually in a probabilistic fashion. Basic to all the models are certain fundamental measures such as mean luminance of the aircraft silhouette as portrayed in aspect, background luminance against which it is presented, and angular size apparent to the searching observer.

Presented in this report are the results of a study to test one particular model for aircraft luminance. Specifically, the model is simply to represent the aircraft as a diffuse (Lambertian) reflecting sphere. This allows a sun angle dependence of sunlit and shadow regions that contribute to total luminance to be included as a first approximation. This representation was combined with surround luminance/atmospheric model to yield a total model for comparison to available photographic data collected in a field test. The surround luminance model includes the ground and sky as sphere illuminators, as well as the direct solar component. The atmospherics account for reduction of illumination according to solar slant path through the total air mass and transport between the aircraft and camera that yielded the data. Although atmospherics were not regarded as very important in the field test, as much detail as possible was included in the analysis to assure it would not be an issue.

The data for model comparison consisted of 16 mm imagery of a low-altitude jet aircraft collected with a camera system corrected to a photopic response. The imagery, which was collected over all azimuths, was supported by radar coordinates of the aircraft such that required geometry would be available. Also included in the imaging were luminance control panels, the luminance values of which were measured simultaneously with film exposure, thereby providing absolute film calibration.

The imagery was analyzed with a scanning two-dimensional densitometer with 16 levels approximately proportional to film transmission. Thus, for

each frame analyzed, frame areas could be measured for each level, which, in conjunction with the calibration data, allowed mean aircraft luminance (apparent at the camera) to be computed.

The data/model comparison yielded significant departure of the data from the model at certain solar phase angles. These data points all possessed sun angle geometry together in the aircraft surface normal directions consistent with solar glint. Other than these data points, a trend of decreasing luminance with phase angle was observed, but weaker than model prediction.

FOREWORD

The work reported herein was performed by Calspan Corporation, Buffalo, New York, under Contract No. DAAK40-75-C-1114 for the U.S. Army Missile Research and Development Command (MIRADCOM), Redstone Arsenal, Alabama. The MIRADCOM technical monitor for this study was Mr. Arthur Poe. The Calspan task leader for this study was Mr. Harry B. Hammill.

Significant contributions by several individuals led to successful completion of this study. These include:

Mr. Arthur Poe, MIRADCOM technical monitor, for many useful and stimulating conversations.

Messrs. William Hyman and Gaylon Branum, MIRADCOM, for execution of flight test photography and collection of calibration photometry.

Mr. Robert Meibaum, EG&G, for cooperation and assistance in film processing to assure special requirements were met.

Mr. Alexander Akerman III, project engineer at inception of the program.

Messrs. George Snider and Thomas Maj for design and fabrication of the camera system.

Mr. Timothy Gallagher for film densitometry.

(This page intentionally left blank)

TABLE OF CONTENTS

Section		Page
1	INTRODUCTION	1
2	DIFFUSE SPHERE MODEL	3
3	FLIGHT TEST	6
	3.1 TEST DESCRIPTION	6
	3.2 PHOTOMETRIC CALIBRATION	7
4	DATA ANALYSIS	8
	4.1 INTRODUCTION	8
	4.2 ANGULAR DATA	8
	4.3 DENSITOMETRY	9
	4.4 MEAN AIRCRAFT LUMINANCE	11
	4.5 APPARENT/INTRINSIC LUMINANCE CONNECTION	16
	4.6 MODEL REGISTRATION	22
	4.7 THE GLINT HYPOTHESIS	27
5	CONCLUSIONS	29
Appendix A	DENSITOMETRY DATA	31
Appendix B	DATA SET FOR MODEL REGISTRATION	36
Appendix C	KOSCHMIEDER'S EQUATION	39

Section 1
INTRODUCTION

The prediction of ranges at which aircraft can be detected visually by ground and airborne observers is of perennial interest. To make such predictions with any degree of confidence, information regarding the intrinsic contrast of the aircraft against its background is required. Because of the multiplicity of types of aircraft, of background against which they might be viewed, of possible lighting distributions, and of the difficulty of measurement of variation in contrast of a target during flight, very little systematic reliable contrast data exists.

This report presents the results of a study to test the validity or appropriateness of one particular mathematical model for aircraft luminance. Visual detection considerations (e.g., the role of resulting contrasts in detectability) were of no concern in the study. Specifically, the approach is one of comparing model prediction to available data to reach a conclusion on model utility.

The model tested is the representation of an aircraft as a diffuse (Lambertian) reflecting sphere for the purpose of computing mean aircraft luminance over the silhouette. Although real aircraft are neither diffuse nor spherical, such a representation does allow some account of the variability with sun angle of the contributions due to sunlit and shadowed regions without undue model complexity. Calspan has in the past used such a model as an indicator of contrast variability to assist in selection of contrast values appropriate as inputs to a visual detection model. Others have also used such a model, in particular, Nagel[1] proposes its use to represent "full form" objects generally, and his paper contains considerable detail.

---

1. M.R. Nagel, "A Model for the Inherent Contrast Conditions in Full-Form Objects," Deutsche Forschungs- und Versuchsanstalt für Luft- und Raumfahrt, D-8031 Oberpfaffenhofen, Germany.

Two sets of data were considered for model comparison: (1) some results from Project COMPASS GHOST in the form of ground-to-air photography of low-altitude jet aircraft, and (2) imagery and support data collected during a flight test by MICOM/USAADS within this study itself. An attempt was made to analyze the COMPASS GHOST imagery, but this was abandoned due to insufficient absolute film calibration.

Included in the sections that follow are a description of the diffuse sphere model, a discussion of the flight test, and a mathematical account of the effects of atmospherics also needed when the comparison is made. Finally, the model/data comparison is made, and conclusions are drawn.

Section 2
DIFFUSE SPHERE MODEL

The details of the application of a diffuse reflecting sphere for predicting aircraft brightness are given in this section. The discussion is limited to the local reflection process; viz., the relationship between flux incident upon the sphere and the reflected flux. Other aspects necessary to ready the model for comparison to field test data, such as brightness propagation through the atmosphere, are included in later sections where appropriate. Finally, it is important to understand that the use of the diffuse sphere here is not the same as saying that, from the viewpoint of visual detectability, the aircraft is modeled as a sphere. It is used only to establish average aircraft brightness with a first-order dependence on sun angle; other detection parameters, such as aircraft size, can be obtained from more appropriate sources.

The average brightness of a diffuse reflecting sphere, as it depends on geometry assuming remote point illumination, has been computed by Russell.[2] We can write:

$$B = \frac{2r\phi}{3\pi^2}\left[\sin\alpha + (\pi - \alpha)\cos\alpha\right] \qquad (1)$$

where r = reflection (visual albedo)

ϕ = sphere illuminance

α = illumination phase angle (apex at sphere)

Clearly, the mean brightness of the sphere due to direct solar illuminance is simply through interpretation of ϕ and α as solar values.

In addition, however, we do not ignore the illumination of the sphere by sky and ground, and an account of these contributions is also included. Only for the purpose of this calculation do we assume the sky and ground to be

2. Russell, H.N., "On the Albedo of the Planets and Their Satellites," Astrophys. J., 43, 3, pp. 179-196, April 1916.

uniform hemispherical illuminators with brightness B_{SKY} and B_{GRD}. For horizontal viewing, conservation and symmetry arguments yield target brightness values due to the sky ($B_{T\,SKY}$) and ground $B_{T\,GRD}$:

$$\left.\begin{aligned} B_{T\,SKY} &= \tfrac{\pi}{2} B_{SKY} \\ B_{T\,GRD} &= \tfrac{\pi}{2} B_{GRD} \end{aligned}\right\} \text{ (horizontal)} \qquad (2)$$

For slant viewing, a dependence on target elevation (ϵ) angle was found by numerical integration of Equation (1), and a good fit is given by:

$$B_T = B_{T\,HORIZ}\left(1 \pm 0.616 \sin\epsilon\right) \text{ (slant)} \qquad \begin{pmatrix} + \text{ GRD} \\ - \text{ SKY} \end{pmatrix} \qquad (3)$$

where the horizontal values ($B_{T\,HORIZ}$) come directly from Equation (2).

The final step to the determination of inherent target brightness is to connect $B_{T\,SKY}$ and $B_{T\,GRD}$ to $\phi_\odot$, our selected common base. First, for the sky, the Handbook of Geophysics[3] conveniently gives ground illumination data broken down into direct solar($I_\odot$) and sky only (I_{SKY}) components as a function of sun elevation. We express these in a theoretical form as:

$$\left.\begin{aligned} I_\odot &= \phi_\odot \sin h_\odot \\ I_{SKY} &= \pi B_{SKY} \end{aligned}\right\} \qquad (4)$$

and therefore,

$$\frac{B_{SKY}}{\phi_\odot} = \frac{\sin h_\odot}{\pi}\left(\frac{I_\odot}{I_{SKY}}\right) \qquad (5)$$

Using the data, numerical evaluation of Equation (5) yields that, for all but the very smallest sun elevations, this ratio is almost constant with a value of 0.045. Thus:

$$B_{SKY} = 0.045\,\phi_\odot \qquad (6)$$

3. United States Air Force, Handbook of Geophysics, MacMillan, 1961.

The ground is now taken to be a diffuse reflector with albedo ρ_G. Both direct sunlight and the sky contribute:

$$B_{GRD} = \rho_G \left(B_{SKY} + \frac{\Phi_o}{\pi} \sin h_o \right) \tag{7}$$

The contribution to inherent target brightness by the diffuse sphere model is now complete.

Section 3
FLIGHT TEST

On 25 February 1976, a flight test was conducted in a desert region by MICOM/USAADS. The purpose of the test was, in part, to collect the data necessary for registration of the diffuse sphere model.

3.1 TEST DESCRIPTION

The test was constructed as four missions, each of which involved several passes of a low altitude jet fighter over a data collection site. The passes covered a variety of approach azimuths in order to provide variable sun angle. Although the passes were close to radial, the natural offsets were sufficiently large that useful data were obtained for aspects other than head-on. Overall, the four missions contained 45 passes.

The resulting test data useful to this study were of three types:

(1) Photographic imagery of aircraft and luminance calibration panels
(2) Radar coordinates of aircraft
(3) Camera operator's log

The prime data, the photographic imagery, was collected on Plus X film with a Calspan-owned system consisting of a Cine-Kodak Special II 16 mm camera with a Century Tele-Athenar 500 mm lens. A Tiffen #11 filter was used to secure a photopic sensitivity. The frame rate (for this test) was set at one per second, and tracking was facilitated by a Redfield 3X-9X zoom riflescope boresighted with the camera. On each pass, photographic recording was initiated as soon as the aircraft was acquired by the camera crew. Usually, the recording ended near crossover, but occasionally, outbound frames were collected.

In addition to the photography, radar coordinates vs time-of-day were provided during each pass at a rate of one per second. Although the camera and radar data rates were the same, they were not actually synchronized. The precision of the radar data was more than sufficient for the needs of the present study.

The camera log contained the detailed flow of the test. Included were camera calibration data, definitions of missions and passes, and comments on the passes where appropiate such as camera start and stop times and estimated number of frames collected.

3.2 PHOTOMETRIC CALIBRATION

Special emphasis was placed on calibration of the camera system to assure that absolute luminance values could be obtained from the film. Prior to the test, a series of exposures was taken over the gamut of exposure times and stops available on the camera. In support of these exposures, source luminance measurements were taken with a Pritchard model 1970 photometer. The resulting film densities could now be related to source luminance, exposure time, and f/number. This relationship, together with a criterion that sky brightness yields film densities in the range of 1.0-1.5, became a rule of thumb for exposure time and f/number setting. Accordingly, at the time of the test, sky brightness measurements near the horizon indicated 1/70-second exposure at f/22. These settings were used throughout the test.

The calibration discussed above was used only for camera setup. The absolute connection between film density and source luminance was obtained by photographing two "field step wedges" located a short distance away from the camera. One wedge faced south and the other north to obtain increased brightness dynamic range according to sun angle. Each wedge consisted of eight sheets of matte paper of differing shades of gray. The sheets, arranged in a 2 x 4 array, had approximate reflectivities of 1.00, 0.70, 0.48, 0.35, 0.24, 0.13, 0.07, and 0.03. Both wedges were photographed at times of opportunity (between missions) in conjunction with remote luminance measurements with the Pritchard photometer of each of the eight steps. These measurements directly provided absolute film calibration, and it is noted that knowledge of reflectivity, such as the values quoted above, is unnecessary.

Section 4
DATA ANALYSIS

4.1 INTRODUCTION

With the exception of the details of this diffuse sphere model (Section 2), all data reduction and analytic procedures are described in this section. This includes reduction of the photographic data (together with merger of appropriate extracts from the radar data) and registration of the diffuse sphere model.

Inherent in the model registration is an account of atmospheric effects. The diffuse sphere model treats only the intrinsic brightness of the aircraft, whereas the photographic data represent apparent brightness according to camera position. Along the path between the two, both atmospheric attenuation and inscattering of light occur, and, to make the connection, a description of these effects is included. Since the purpose of the investigation is a test of the diffuse sphere model, as much detail as possible was included on atmospherics to eliminate it as an issue. Accordingly, some of the following subsections become rather involved with atmospherics, but the reader should not conclude from this that atmospheric effects are correspondingly important. Actually, visibility during the test was excellent, and the photographic ranges were short. Although atmospherics did affect luminance values, it was not a major factor.

4.2 ANGULAR DATA

Both the diffuse sphere and the atmospheric models require certain angular data as inputs. As a matter of convenience, for each data point in the radar record, aircraft azimuth and elevation, sun azimuth and elevation, and solar phase angle (angle between the sun and camera with apex at the aircraft) were computed and made available as a data-set. Later in the analysis, extracts from these data are merged with the photographic data.

4.3 DENSITOMETRY

The first step in the analysis of the film data is the reduction of the photographic images of aircraft and sky to suitable numerical form. To accomplish this, use was made of a two-dimensional scanning densitometer manufactured by Spatial Data Systems. This instrument consists of a closed-circuit television system with the ability to provide values proportional to total areas within the scanned field that lie within predetermined brightness values. Thus, by providing the TV sensor with a light table and appropriate optics, individual 16 mm frames were scanned and the image dichotomized into a sequence of numbers representing areas within the frame corresponding to neighboring density increments of the film.

The brightest level, the darkest level, and the number of steps between are degrees-of-freedom of the densitometer, and their selection entailed examination of the film data in advance of the final measurements. It was therefore determined that one of the frames containing a brighter (south-facing) image of the eight-step field wedge was satisfactory for calibration, and a procedure for "locking on" the wedge with the brightest and darkest levels was established.

By trial, it was found that 16 bands or density increments between the two limits could be included for measurement without undue hardship. In regard to the increments, two comments are appropriate. First, the densitometer allows the selection of the scaling of these increments to be linear (approximately) with either film density, which varies as the log of film transmission, or transmission itself. Since our interest will be in averaging over scene luminance, which relates closely to film transmission, the latter mode was employed. Secondly, a valuable adjunct to the densitometer is a monitor which displays the scanned image, with the sequence of transmission increments appearing as individual false colors. This is especially useful for identification of areas within the aircraft silhouette that fall within the same brightness increment as the sky (or terrain) present in the frame. In these cases, since the regions involved external to the aircraft image consume large areas of the frame, the area measures for those increments are contaminated beyond use. In all cases where this occurred, visual estimates were made of the

percent of silhouette area for each increment involved. The incorporation of these estimates into the analysis will be discussed later.

The calibration was completed by meshing the photometer-measured luminance values for the eight-step wedge and the 16 increments to be used for data reduction.* The results of this yielded a luminance schedule for the increments as follows:

Increment	Luminance (ft-L)	Increment	Luminance (ft-L)
1	50	9	1600
2	180	10	1890
3	270	11	2190
4	370	12	2550
5	500	13	2980
6	700	14	3730
7	990	15	4500
8	1280	16	5260

The luminance values represent the centers of the increments.

For each pass containing usable imagery, one of the frames near crossover was selected as number one in an ad-hoc frame-numbering sequence, with frame number increasing with successive earlier frames, i.e., backward on the film strip. Since the imagery was usually of the aircraft while inbound, increasing numbers meant greater range and correspondingly smaller image size. Successive frames were analyzed in increasing number until either camera acquisition was reached, or resolution became a problem. The results of this analysis were punched on IBM cards to be available as data for the next data reduction stage. Each frame analyzed was represented by one card containing pass number, frame number, area measures (or % areas) for the 16 increments, increment number for the sky near the aircraft, and the increment number for terrain if present in the frame. A printout of these data is given in Appendix A.

*For calibration only, 32 increments were actually used to obtain increased luminance resolution.

4.4 MEAN AIRCRAFT LUMINANCE

The diffuse sphere model described in Section 2 predicts average luminance of the spherical silhouette. Since we have no specific interest in the luminance structure, the mean of the data can be computed now. Although the data represent aircraft luminance apparent to the film and the model represents intrinsic luminance of the aircraft, corrections for atmospherics and camera flare (anticipated here) can be treated independently. That is, the triad of operations:

(1) computation of silhouette mean luminance
(2) correction for atmospherics
(3) correction for flare

are all processes obeying the principle of linear superposition and can be freely transposed.

An expression for the mean, accounting for estimated percentages in the absence of measured areas, is now derived. The mean luminance ($\bar{B}$) is written:

$$\bar{B} = \frac{\sum_{i=1}^{N} a_i B_i}{A} \tag{8}$$

where:

$$A = \sum_{i=1}^{N} a_i \tag{9}$$

The summations are, of course, over the N non-zero increments of the data in Appendix A. For our purpose here, let the first M components of the summations be the measured areas, and the components M+1 to N, estimated percentages. Equation (8) is now expressed:

$$\bar{B} = \frac{1}{A}\left(\sum_{i=1}^{M} a_i B_i + \sum_{j=M+1}^{N} a_j B_j\right) \tag{10}$$

or:

$$\bar{B} = \frac{1}{A} \sum_{i=1}^{M} a_i B_i + \sum_{j=M+1}^{N} f_j B_j \tag{11}$$

where f_j is an area fraction. Similarily, Equation (9) becomes:

$$A = \sum_{i=1}^{M} a_i + A \sum_{j=M+1}^{N} f_j \tag{12}$$

Eliminating A between Equations (11) and (12) yields:

$$\bar{B} = \left(1 - \sum_{j=M+1}^{N} f_j\right) \frac{\sum_{i=1}^{M} a_i B_i}{\sum_{i=1}^{M} a_i} + \sum_{j=M+1}^{N} f_j B_j \tag{13}$$

which is the final expression to be used.

Before leaving the concept of incorporating estimated percentages, a comment is in order regarding the stability of $\bar{B}$ on errors in estimation. We note that for a small unknown a_j, the estimate f_j has high relative error. However, since the contribution to $\bar{B}$ is correspondingly small, no instability occurs. On the other hand, as a_j and f_j become large, the relative error of f_j becomes small. Although absolute errors in f_j (when a_j is large) cause large relative errors in the contributions of the measured a_i's, they are themselves small, and again, no instability occurs. On one frame (pass 27, frame 12), it was necessary to estimate all non-zero increments, but the resulting mean luminance was nonetheless acceptable.

At this point, some emending of the film data was necessary. Due to low offset values, high angular rates were possible near crossover, thereby indicating a high time resolution requirement for camera/radar data synchronization. Since it was indicated in the camera log that camera times near the end of the passes were of questionable accuracy, they were not employed. Instead, the film was previewed to locate crossover, a matter of visual aspect of the aircraft engine exhaust port. Since the frame nearest crossover became

the key to synchronization with the radar data, all passes that did not contain crossover imagery were deleted from further analysis. In addition, anomolous low luminance values were noted from the densitometry of passes 36 through 42, and these were deleted as well.

The surviving data were analyzed according to Equation (13), and, as a matter of general interest, apparent contrast (C) of the aircraft according to:

$$C = \frac{\bar{B} - B_s}{B_s} \tag{14}$$

was computed as well. B_s is selected from the schedule in section 4.3 according to the sky brightness increment number. By means of identifying the crossover frame within the frame scale for each pass, the radar and camera data were synchronized. This allowed $\bar{B}$ and the associated geometry parameters necessary for model registration to be merged. The merged data were punched on IBM cards, with one card again representing one frame, as follows:

(1) Pass number
(2) Frame number
(3) Number identifying radar data point
(4) Slant range (meters)
(5) Aircraft elevation angle (degrees)
(6) Solar elevation angle (degrees)
(7) Solar phase angle (degrees)
(8) Sky luminance (ft-L)
(9) $\bar{B}$, mean apparent aircraft luminance (ft-L)

A printed list of this data set is included in Appendix B. The printed version includes the resulting apparent contrast values as well.

In anticipation that solar phase angle is the dominant independent variable of the diffuse sphere model, the mean illuminance data were simply plotted against phase angle. The result is shown in Figure 1, and three observations are made:

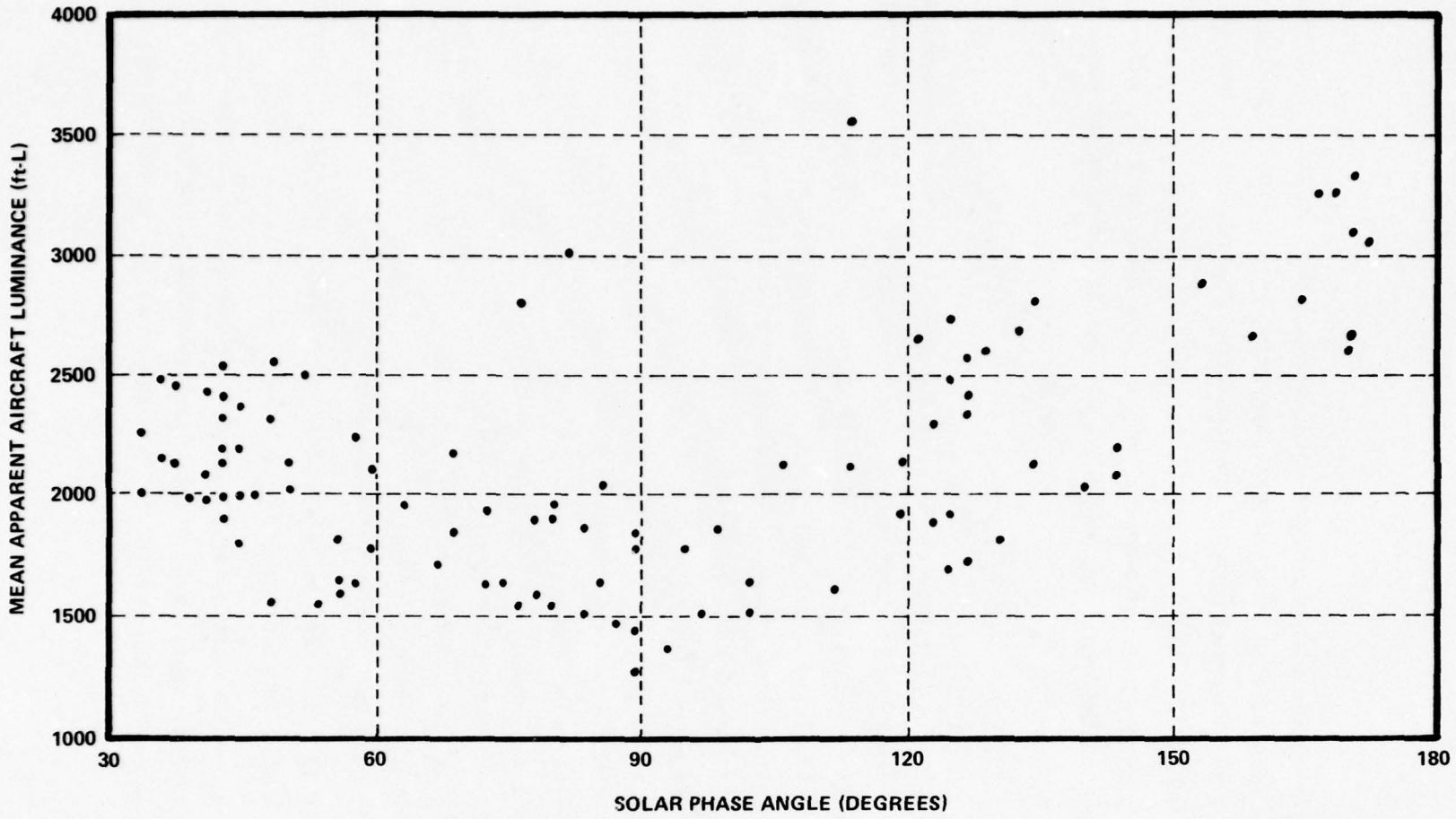

Figure 1 Quick Look at Mean Luminance Values

(1) At angles less than 90°, the decreasing luminance with increasing angle is consistent with the model, although the slope is less than anticipated.

(2) At angles greater than 90°, the increasing luminance with increasing angle is in direct opposition to the model since the model luminance is monotonic in phase angle.

(3) In the mid-range of phase angle, three data points lie significantly above the main trend.

In regard to (3), it was suspected that solar glints were responsible. Glint is loosely defined here as those singularly intense specular reflections from surfaces that are close to being either flat or conical. (It is noted that the skin of the aircraft is unpainted metal and specular reflections can be expected.) The three frames involved (pass 3, frame 2 and pass 23, frames 4 and 5) did indeed contain significant glint and were not included in the model registration. However, the occurrence of these glints will not be ignored in the final evaluation of the model.

The departure indicated in (2) has major significance. If it does not represent a failure on the part of the diffuse sphere model, it must be due to a mechanism that causes aircraft luminance apparent at the film to differ from inherent aircraft luminance in a fashion consistent with the data, and two candidates can be identified:

(1) Camera flare from direct solar irradiance

(2) Strong forward scattering by the atmosphere (i.e., Mie scattering by haze)

Thus, it is critical to the resolution of the question of the departure at large phase angles that both these mechanisms be accounted for at the time of model registration, and this forms the subject of the following section.

4.5 APPARENT/INTRINSIC LUMINANCE CONNECTION

We now address the connection between apparent and intrinsic aircraft luminances in terms of camera flare and atmospherics that have been identified as accountable mechanisms prior to model registration.

For flare, the camera system underwent laboratory measurements to determine film plane irradiance as a function of phase angle. Scaling to the flight test illumination levels was accomplished through the luminance value measured for one of the steps in the field calibration wedge and, accounting for sun angle, an equivalent laboratory simulation. The measurements show flare can be neglected for angles less than 165°. For angles increasing above 165°, flare increases very rapidly, reaching 580 ft-L at 172°. The accuracy of the laboratory data, both in angle and source collimation, precluded attempts to provide a phase-angle-dependent flare correction. Accordingly, deletion of data at these high angles (passes 44 and 45) from model registration eliminated camera flare as a factor.

The remainder of the discussion here presents a mathematical system for handling the optical effects of the atmosphere. Although the system may appear relatively involved, it does not necessarily mean that atmospherics are important. It only means the descriptive tools were readily available, and to identify and sift out those that would be unimportant seemed pointless. As a matter of hindsight, atmospherics did not turn out to be the prime factor in model registration.

The atmosphere has two distinct optical effects beyond the illumination scheme discussed in Section 2. First, propagation of luminance follows a transport equation involving atmospheric parameters for points along the path between the aircraft and camera, and, second, the low-altitude illuminance ϕ [which appears in Equation (1) as well as below] is reduced according to solar elevation angle through the total air mass above the earth.*

*The reader not specifically interested in details of atmospheric effects can proceed to the last sentence before section 4.6, and continue.

The propagation will be handled here by a standard form of the transport equation known as Koschmieder's Equation:*

$$B = B_0 e^{-\tau} + B_\infty (1 - e^{-\tau}) \tag{15}$$

where: B_0 = inherent luminance of aircraft

B = aircraft luminance apparent at the camera

τ = optical thickness of aircraft/camera path

B_∞ = atmospheric "equilibrium" luminance

The conditions of validity are that, over the path in question, both the solar irradiance and the shape of the scattering coefficient (phase function) are stationary. Since the aircraft elevation is low (usually a few hundred meters) and atmospherics is not expected to be a major factor, variability of atmospheric properties over the path will not be addressed.

In Equation (15), the optical thickness is simply:

$$\tau = \beta R \tag{16}$$

where: β = attenuation coefficient (m^{-1})

R = aircraft/camera slant range (m)

with β in turn given by the definition of meteorological range (V):

$$\beta = \frac{\ln 50}{V} \tag{17}$$

*The terminology used here and in the equations that follow are standard. For further details, the equation is derived from a more general form in Appendix C, which includes definitions and validity conditions. Beyond this, any number of texts can be found. Middleton is especially lucid.

The equilibrium luminance, β_∞, is given by the spherical integral:

$$\beta_\infty = \oint \hat{k} B_{SUR} \, d\Omega \tag{18}$$

where: $\hat{k}$ = phase function at path point

B_{SUR} = spherical luminance function surrounding path point

and the integration is over 4π steradians about the point. To obtain the phase function, we recognize two independent physical scattering mechanisms: scattering by atmospheric density fluctuations on a molecular scale (Rayleigh scattering) and scattering by water haze (Mie scattering). The form for Rayleigh scattering ($\hat{k}_R$) is well-known[4]:

$$\hat{k}_R = \frac{3}{16\pi}(1 + \cos^2\gamma) \tag{19}$$

where γ is the scattering angle. (For the direct sunlight component, γ is simply $\pi - \alpha$, the phase angle.) The phase function is very much different for Mie scattering ($\hat{k}_M$). Data given by Deirmendjian[5] can be expressed by a simple model:

$$\hat{k}_M = 10^{0.73 - 2.9\gamma + 0.68\gamma^2} \tag{20}$$

with γ expressed in radians. A plot of $\hat{k}_M$ vs γ in degrees is given in Figure 2, and very strong scattering in the forward direction is evident. This is precisely the effect described earlier as being important that it not be overlooked as a possible explanation for the trend of the data at high solar phase angles.

4. S. Chandrasekhar, Radiative Transfer, Dover Press (1960)

5. D. Deirmendjian, Electromagnetic Scattering on Spherical Polydispersions, Elsevier Publishing Co. (1969).

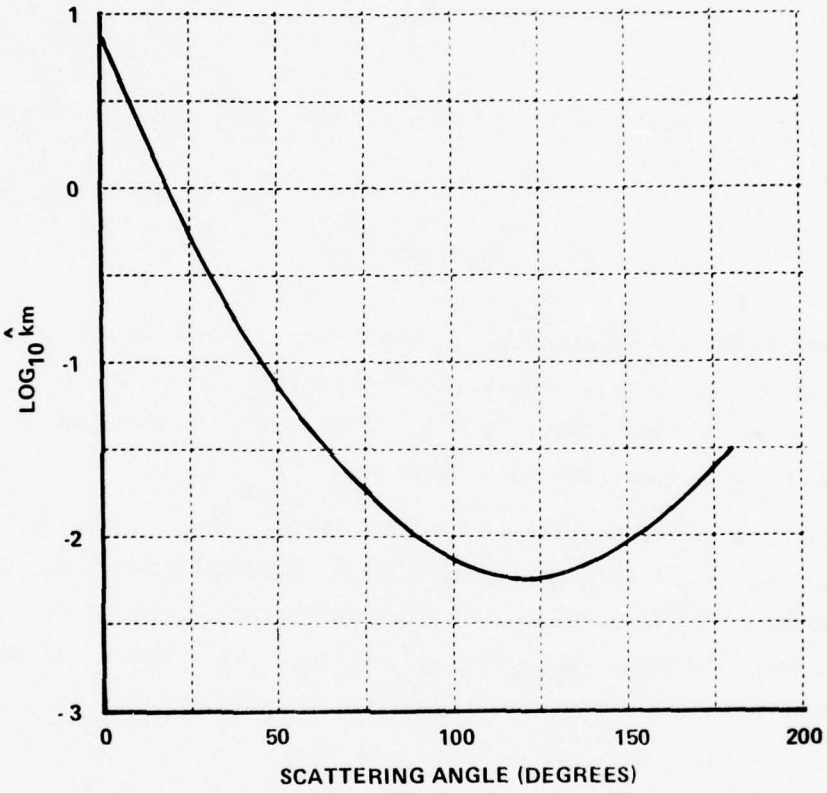

Figure 2 Phase Function Model for Scattering by Haze

With the individual scattering mechanism described, the resultant phase function $\hat{k}$ required by Equation (18) is given by the weighted superposition of the components:

$$\hat{k} = \frac{\beta_R \hat{k}_R + \beta_M \hat{k}_M}{\beta} \tag{21}$$

where β_R and β_M are the individual Rayleigh and Mie scattering coefficients which satisfy:

$$\beta = \beta_R + \beta_M \tag{22}$$

The Rayleigh scattering coefficient, β_R, is a constant, and we will give its value below along with other constants. The Mie coefficient, which is proportional to haze concentration, is a variable, and its value is found from Equation (22) in conjunction with Equation (17).

We now turn our attention to the completion of the spherical integration of Equation (18). Through a piecewise breakdown of the integrand and a few approximations, a simple algebraic expression for β_∞ can be obtained. First, the surround luminance, B_{SUR}, can be written as the sum of direct sunlight $B_\odot$ and a residual diffuse part B_{DIF}:

$$B_{SUR} = B_\odot + B_{DIF} \tag{23}$$

and Equation (18) becomes:

$$B_\infty = \oint \hat{k} B_\odot \, d\Omega + \oint \hat{k} B_{DIF} \, d\Omega \tag{24}$$

Since $B_\odot$ is bounded to the solar disc, which has a subtense only 1/2° in diameter, $\hat{k}$ is constant and assumes a value ($\hat{k}_\odot$) according to the solar phase angle. We can now write:

$$\oint \hat{k} B_\odot \, d\Omega = \hat{k}_\odot \oint B_\odot \, d\Omega = \hat{k}_\odot \phi_\odot \tag{25}$$

where $\phi_\odot$ is the direct solar irradiance. In regard to the diffuse part of Equation (24), a further expansion is obtained through the separate scattering mechanisms. Elimination of $\hat{k}$ between Equation (21) and the diffuse term yields:

$$\oint \hat{k} B_{DIF} \, d\Omega = \frac{1}{\beta} \left(\beta_M \oint \hat{k}_M B_{DIF} \, d\Omega + \beta_R \oint \hat{k}_R B_{DIF} \, d\Omega \right) \tag{26}$$

Now, since $\hat{k}_M(\gamma) \sin\gamma$ is concentrated at small γ as well as $\hat{k}_M(\gamma)$, the main contribution to the first integral in Equation (26) is from B_{DIF} in the vicinity of $\gamma = 0$. We therefore make the approximation that B_{DIF} is a constant equal to the sky brightness, B_S, extracted from the film. Thus:

$$\oint \hat{k}_M B_{DIF} \, d\Omega = B_S \tag{27}$$

The final integral, the diffuse term of Equation (26), possesses an integrand whose dependence on γ is very weak. Ignoring the ground as a contributor, B_{DIF} is replaced with a representative mean value for the sky and, for this purpose, the value B_{SKY} [Equation (6), Section 2] is used. Therefore, we have:

$$\oint \hat{k}_R B_{DIF} \, d\Omega = \frac{1}{2} B_{SKY} \tag{28}$$

and the integration to yield B_∞ is complete. Collecting all the pieces, Equation (18) is finally written:

$$B_\infty = \left[\hat{k}_\odot + 0.0225 \left(\beta_R / \beta \right) \right] \phi_\odot + \beta_M B_S \tag{29}$$

What now remains, to complete the connection between apparent and intrinsic aircraft luminance, is a procedure for generating $\phi_\odot$, and the specification of some left-over constants. The parameter $\phi_\odot$, used both here and in Section 2, is direct solar illuminance (perpendicular to sun direction)

at ground level. As the elevation angle of the sun is reduced, $\phi_{\odot}$ decreases due to an increased path through the atmosphere according to:

$$\phi_{\odot} = \phi_{\odot\odot} e^{-\frac{\tau^*}{\sin h_{\odot}}} \tag{30}$$

where $\phi_{\odot\odot}$ = solar illuminance outside atmosphere

τ^* = vertical optical thickness of air mass

$h_{\odot}$ = solar elevation angle

From an atmospheric model by Elterman[6], τ^* can be found:

$$\tau^* = 0.147 + \frac{5000(\beta_M - \beta_5)}{\ln(\beta_M/\beta_5)} \tag{31}$$

The parameter β_5 is the Mie scattering coefficient at an altitude of 5000 meters, a pivot point in this model. The value for β_5, as well as the value for β_R needed in earlier equations, are given by Elterman as:

$$\begin{aligned} \beta_5 &= 5.02 \times 10^{-6} \text{ meters}^{-1} \\ \beta_R &= 1.162 \times 10^{-5} \text{ meters}^{-1} \end{aligned} \tag{32}$$

The connection between apparent and intrinsic aircraft luminance is now complete to within the two parameters, V (meteorological range) and $\phi_{\odot\odot}$ (a number for solar illuminance).

4.6 MODEL REGISTRATION

The atmosphere description, together with the diffuse sphere model of Section 2, form the total model for registration on the data. Overall, four parameters remain unspecified:

6. L. Elterman, "UV, Visible, and IR Attenuation for Altitudes to 50 KM, 1968", AF Cambridge Research Laboratories, AFCRL-68-0153 (April 1968).

(1) ρ, aircraft reflectance (albedo)

(2) ρ_G, ground reflectance (albedo)

(3) ϕ_{oo}, solar illuminance external to atmosphere

(4) V, meterological range (meters)

Reflectance values for a variety of terrains are given by Gorden and Church[7]. From these, a value of 0.22 ("Dirt - flat desert road freshly bulldozed") was assigned to ρ_G. The remaining three parameters were varied in initial attempts to effect a model/data fit.

The criterion for registration was to minimize the total square error in apparent aircraft luminance by means of a global search in the space of the adjustable parameters. Such a search over the space of ρ, ϕ_{oo}, and V did not converge to a reasonable solution. Apparently, the Mie scattering mechanism, although having a proper phase angle dependence as noted earlier, was too weak at normal meteorological ranges; and, to compensate, the registration increased β_M, thereby driving V to an extremely small value.

For proper registration, it became necessary to specify both V and ρ and to leave ϕ_{oo} as the only variable. A value of 40 km was selected to be as low as the writer was willing to use in light of the observation that visibility during the test was "very high." Should atmospherics remain an issue, further consideration would be given to V as required.

The surface of the aircraft was primarily (but not entirely) unpainted metal, and a value of 0.7 was chosen for ρ. This is moderately less than the visual albedo for aluminum. The importance of the reflectance value, again, is related to the importance of the atmospherics. An error in reflectance will in part be compensated for by ϕ_{oo} during registration since intrinsic aircraft luminance is proportional to the product $\rho\phi_{oo}$. The compensation is not complete because ϕ_{oo} affects apparent luminance through inscattering, whereas ρ does not. Thus, if inscattered light between the aircraft and camera

7. J.I. Gorden and P.V. Church, "Directional Luminous Reflectances of Objects and Backgrounds for a Moderately High Sun," Contained in S.Q. Duntley et al., "Visibility," University of California Scripps Institute of Oceanography.

is not important, neither is aircraft reflectance. We shall treat ρ in the same fashion as V, in that further consideration of its value will be given if necessary.

Model registration was completed through adjustment of the lone parameter ϕ_{oo}. The completed model was then exercised using as input all necessary data corresponding to each measured apparent luminance value, to yield predicted apparent luminances on a one-for-one basis. The resulting data/model luminance pairs are plotted in (a) and (b) of Figure 3 against solar phase angle. (The division into two plots was only to facilitate presentation of the large number of points; no distinction between the missions is intended.) From these plots, the following observations are made:

(1) In the range of 0-90°, the trend of decreasing luminance with phase angle is present in the data but is weaker than the model predictions.

(2) At angles greater than 90°, significant departures occur between the data and the model. Since forward scattering by haze was not significant, the departures are considered real, in that they are present in the intrinsic luminance as well as the apparent luminance.

(3) The overall departure of the model from the data is much greater than deviations within the model at any given phase angle. Since these deviations contain atmospheric effects along the slant path between the aircraft and camera, atmospherics can be regarded as unimportant. Thus, the selection of values for meteorological range and aircraft reflectance need not be redressed.

(4) In regard to deviations within the model, two model points lie below 2000 ft-L at small phase angles on (b) of Figure 3. These two points occurred on pass 35 with a solar elevation angle of only 19°, and significant downward correction in aircraft illuminance resulted from attenuation by the total air mass.

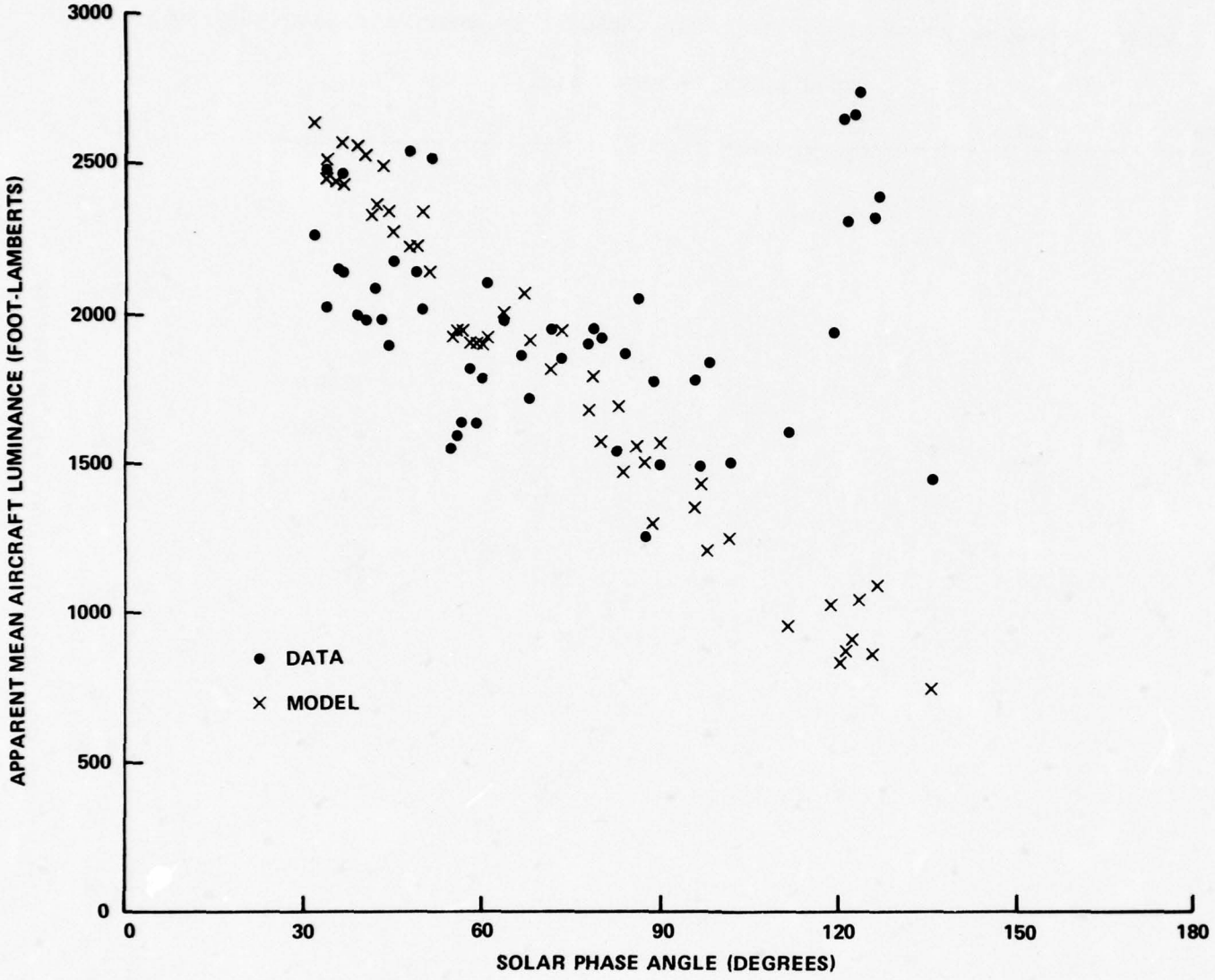

Figure 3(a) Aircraft Luminance vs Phase Angle – Data/Model Pair Comparison for Missions 1 and 2

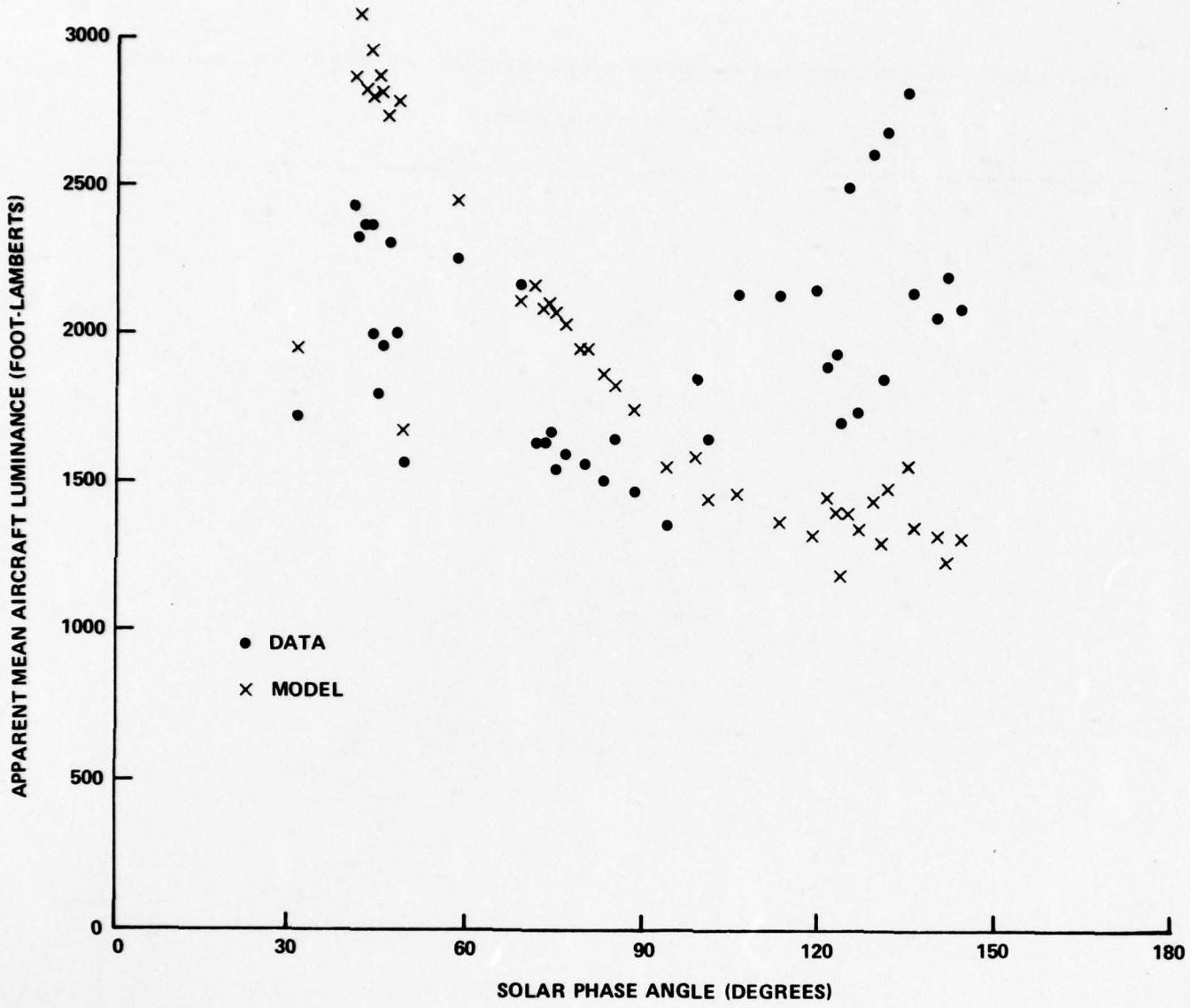

Figure 3(b) Aircraft Luminance vs Phase Angle – Data/Model Pair Comparison for Missions 3 and 4

4.7 THE GLINT HYPOTHESIS

This section concludes with the suggestion that glint is likely responsible for the principal model/data departure. Although inconclusive, the question of whether or not the geometry is correct for glints to occur can be answered approximately. To do this, a sufficient first order description of the aircraft is as follows:

(1) Wings - horizontal flats

(2) Tail - vertical and horizontal flats

(3) Fuselage - cylinder

Although the wings are an unlikely source of glint, all surfaces as represented above have surface normals at 90° to the forward axis of the aircraft. Since specular reflections occur when the solar phase angle is bisected by the surface normal, the data we have can be put to a test. Thus, for all the data, the angle between the phase angle bisector and the forward direction of the aircraft was computed and plotted against phase angle itself (Figure 4). The encircled points are those in Figure 3 having the large departures from model prediction. They primarily fall in the range of 100-110° aft of the forward direction, with some at 120°. Thus, there is an excellent agreement between the phase angle bisector and normals to aircraft surfaces that we would expect to be responsible for glint. This is regarded as strong evidence that the primary departure between the data and the model is due to glint.

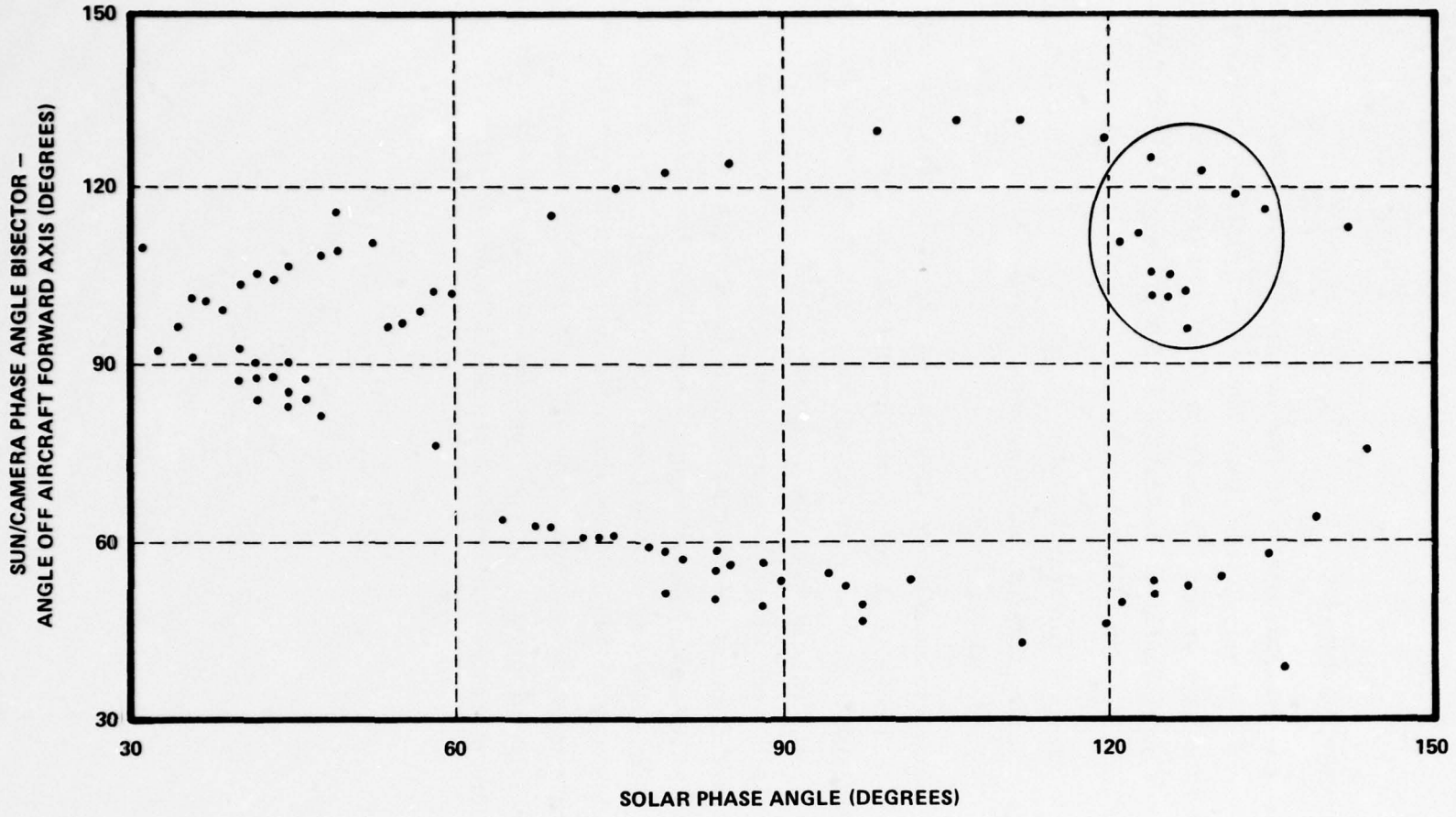

Figure 4 Connection Between Phase Angle Bisector Direction and Phase Angle

Section 5
CONCLUSIONS

The prime result of this study was the registration of a diffusely reflecting sphere model for predicting aircraft luminance on field test data, and the resulting comparison was shown in Figure 3. The question of whether or not the model is valid or appropriate requires a highly qualified answer. It depends on the accuracy required in application, the nature of the use of the results, and the availability or appropriateness of alternate models.

For example, the model should probably not be used when sun angle is a critical issue. On the other hand, applications that only require a measure of variability due to sun angle may find the model useful. The answer as to whether or not the model is appropriate must come from the user.

Probably the greatest limitation of the model is the availability of significantly better models not much more complex. The crude geometrical representation of the aircraft given in Section 4.7, or something akin to it, could be the basis of a different model resulting in a much better fit to the field data. The fact that the aircraft used in the test was neither diffuse nor a sphere is not a fault of the model, since its use was strictly empirical. However, by including a little attention to the actual surface shape, and the reflective properties, improvements probably will occur. It is noted that optical reflection signatures for diffuse and specular flats, cones, and cylinders, and compound surfaces such as spheres are known, and a replacement for the diffuse reflecting sphere seems very close at hand.

(This page intentionally left blank)

Appendix A

DENSITOMETRY DATA

Included here are the raw data for aircraft brightness resulting from the densitometery analysis of the flight test imagery. The first two columns contain the pass number and camera frame number, respectively (P/F). The next 16 columns contain the actual areas of the aircraft image (arbitrary units) that fall within each of the 16 brightness increments employed in the dichotomy. For those increments that could not be measured due to contamination from regions external to the aircraft silhouette, percentage estimates of total silhouette area were made and labeled negative for identification. The last two columns are the brightness bin numbers for the sky (S) and typical terrain (T) when present in the frame.

The meaning and use of all data in the following table are discussed in detail in the main text.

TABLE A-1. RAW DATA FROM DENSITOMETER ANALYSIS

P	F	LUMINANCE INCREMENT AREAS (ARBITRARY UNITS) 1	2	3	4	5	6	7	8	9	10	11	12	13	14	15	16	S	T
1	8										.1	.3						12	
1	7									.1	.2							12	
1	6					.02	.03	.02	.03	.1	.3							12	
1	5									.2	.6							12	
1	4							.1	.3	.5	.8							12	
1	3					.05	.05	.3	.5	.9	1.5							11	
1	2						.5	.8	1.2	1.8	3.4							11	
2	5											.2	1.1	-5.				13	
2	4											.2	1.3	-10.				13	
2	3										.1	.3	1.2	-15.				13	
2	1									.3	.3	.6	1.8	-5.	-10.			14	
3	6											.1	.2	-3.	-20.	-2.		14	
3	5										.1	.2	.3	-5.	-15.	-5.		13	
3	4						.2	.3	.2	.3	.3	.4	.5	-3.	-5.	-15.		13	
3	3									.4	.5	.5	1.3	-3.	-5.	-15.		13	
3	2								.1	.4	.8	1.6	-10.	-10.	8.9	7.2		12	
4	7						.02	.03	.02	.03	.3	.3						12	
4	6						.03	.03	.03	.2	.4	.4						12	
4	5					.03	.03	.03	.2	.6	.5	.5						13	
4	4						.03	.03	.03	.8	.7	.7						13	
4	3			.02	.03	.02	.03	.4	1.8	1.4	1.1	1.1						13	
4	2						2.2	2.9	3.4	2.8	1.9	3.1						13	
5	7										.1	.5						12	
5	6											.6						12	
5	5									.1	.1	.6						12	
5	4										.2	.6	-5.					12	
5	3								.1	.1	.3	.9						12	
5	2								.1	.3	.8	2.5	-20.					12	
5	1									.4	1.3	-20.						13	
6	6										.1	.2	.3	-10.	-15.			14	
6	5						.04	.04	.04	.04	.04	.1	.2	-10.	-15.			14	
6	4										.1	.3	.4	-10.	-15.			14	
6	3						.03	.03	.03	.2	.4	.5	.7	-15.	-10.			13	
6	2								.3	.6	.6	1.1	-10.	-35.				12	
8	3							.1	.1	.1	.3	.6	1.8	-5.	-10.			13	
8	1							.1	.3	.3	.4	1.4	-10.	-10.	-10.			13	
9	8									.1	.3	.3						12	
9	7								.1	.5	.6							12	
9	6								.1	.6	.8	1.4						12	
9	5								.1	.8	.9	1.1						12	
9	4								.4	1.2	1.2	.9	1.9					13	
9	3								1.1	1.6	1.8	1.5						13	
9	1							.4	1.3	2.3	2.4	2.3	2.6					13	
10	6									.1	.1	.2	.5	-30.				13	
10	5										.1	.1	.5	-40.				13	
10	4										.2	.2	.3	-40.				13	
10	3								.1	.2	.3	.6	1.5	-2.	-3.			14	
11	4										.4	.3						13	
11	3									.1	.5	.4						13	
11	2									.1	.7	.6						13	
11	1									.2	.9	.8						13	
13	11										.3	.3						12	
13	10									.1	.4	.4						12	
13	9									.2	.5	.6						13	

TABLE A-1. (Cont.) RAW DATA FROM DENSITOMETER ANALYSIS

P	F	LUMINANCE INCREMENT AREAS (ARBITRARY UNITS) 1	2	3	4	5	6	7	8	9	10	11	12	13	14	15	16	S	T
13	7										.7	1.0						13	
13	6							.2	.6	1.3	1.2							11	
15	6							.1	.8	.8	.6							12	
15	5				.03	.03	.03	.7	1.2	1.1	1.0							12	
15	4							.7	1.2	1.2	1.3							13	
17	6						.1	.8	1.2	.8								11	
17	5					.6	1.2	1.1	1.1									10	
17	4						1.2	1.3	1.7	1.7	2.4							12	
17	3						.6	2.0	2.2	2.4	2.5	2.5						12	
18	9						.03	.03	.03	.1	.2	.3						12	
18	8					.05	.05	.05	.05	.1	.3	.6						12	
18	7			.02	.02	.02	.02	.02	.2	.4	.6	2.0						12	
18	6						.3	1.6	1.8	1.7								10	
18	5			.1	.1	.1	.2	1.5	2.6	2.8	4.3							11	
19	3									.01	.01	.01	.01					13	
19	7							.03	.03	.03	.1	.1						12	
19	6							.03	.03	.03	.1	.7						12	
19	5							.03	.03	.03	.2	.3						12	
19	4							.2	.1	.1	.3	.5	2.1	-5.				13	
19	3									.1	.5	.6	.7					14	
19	1				.2	.1	.1	.4	1.2	1.2	1.6	1.8						12	
22	9											.1	.2					13	
22	8											.2	.4					13	
22	7											.3	.3					13	
22	6											.5	.5					13	
22	5										.1	.8	.6					13	
22	3										1.0	1.1	1.4					13	
23	5												.2	-15.	-35.			14	
23	4											.1	.2	-10.	-20.	-30.		12	
23	3								.3	.3	.4	-1.	-10.	-10.	-15.			12	
24	7							.03	.03	.03	.2	.2						12	
24	6							.03	.03	.03	.3	.4						12	
24	5									.2	.4	.7						12	
24	4								.5	.9	1.1							12	
24	3								.6	1.4	1.9	1.9						12	
24	2							.5	1.2	2.5	2.7	2.5	3.1					13	
25	8											.1	-15.					13	
25	7										.1	.2	-15.					13	
25	6					.02	.02	.02	.02	.02	.2	.5	-15.					12	
25	5					.02	.03	.02	.03	.2	.6	1.0	-10.					12	
25	4								.3	.8	1.0	1.6	-10.					12	
26	9										.1	.3	-25.	-15.				12	
26	6								.4	.5	.8	2.5	-8.	-10.	-10.			12	
26	5							.3	.8	.8	.9	-3.	-5.	-5.	-15.			12	
26	4								.4	.7	1.1	-5.	-5.	-15.	-5.	9.6	5.6	11	
27	12								-5.	-30.	-15.							12	10
27	11								.1	.4	.3							12	
27	10							.1	.3	.4	.3							12	
27	9							.1	.2	.5	.4							12	
27	8							.1	.5	.6	.5							12	
27	7						.1	.1	.7	.9	.5							12	
27	6					.1	.1	.4	.9	1.2	.9							12	
27	5				.1	.1	.3	1.7	1.7	1.3	1.6							11	
27	4							1.4	1.5	2.1	2.4	1.7						12	

TABLE A-1. (Cont.) RAW DATA FROM DENSITOMETER ANALYSIS

P	F	LUMINANCE INCREMENT AREAS (ARBITRARY UNITS) 1	2	3	4	5	6	7	8	9	10	11	12	13	14	15	16	S	T
27	2					.1	1.4	3.0	4.0	4.6	3.6	3.3	4.2					14	
29	8												.6	1.0				14	
28	7											.2	1.0	.8				14	
28	6											.2	1.3	-10.	-5.			14	
28	5										.1	1.1	2.1	-5.	-5.			14	
28	4									.4	1.5	1.9	-25.	-1.				13	
28	3									.4	1.7	2.3	-20.					13	
28	2										2.0	2.6	-15.					13	
28	1								.2	2.7	3.3	2.3						13	
28	-2								1.4	2.5	2.5							12	
28	-3								.2	1.6	2.9	4.3						12	
28	-4						.1	.2	1.5	1.8	3.1							12	
29	7											.1	-30.	-5.	-45.			13	
29	6										.1	-10.	-5.	-40.				13	
29	5											.1	.6	-5.	-15.	-30.		13	
29	2										.3	.6	-15.	-35.				13	
30	14											.2	.3					14	
30	13										.1	.2	.3					14	
30	12											.3	.3					14	
30	11										.2	.3	.5					14	
30	10									.1	.5	.4	.6					14	
30	9									.2	.9	.5	.7					14	
30	8								.1	.7	1.2	.5	.7					14	
30	7							.1	.3	.9	1.7	.7	.9					13	
31	7										.1	.4	.8	-15.	-10.			14	
31	6										.3	1.0	1.0	-5.	-15.			13	
31	5						.1	.1	.1	.3	.8	1.3	1.4	-10.	-15.			13	
31	4								.1	.6	1.0	1.3	1.5	-10.	-15.			13	
31	3										.5	1.1	1.4	-15.	-15.			13	
31	1								.4	1.5	2.0	2.5	5.6	-20.				13	
32	5							.2	.7	1.0	1.8	1.4						13	
32	4								.3	1.2	1.7	2.3	-12.					12	
33	9									.2	.3	.2						13	
33	8									.2	.3	.3						13	
33	7								.2	.7	.3	.3						13	
33	6								.2	.7	.5	.5	-5.					13	
33	5								.1	.8	1.0	1.0	1.8					14	
33	4								.1	1.1	1.8	1.2	1.5					14	
33	3									1.0	1.4	1.1	1.4					14	
33	1								1.2	3.6	3.8	3.1	3.7	4.1				14	
35	3				.2	.8	1.2	1.0	1.7	-5.	-20.	-20.	-10.					11	
35	2			.3	1.2	1.2	.9	1.6	2.6	3.7	-5.	-10.	-20.	-10.				10	
36	9	.9																10	5
36	8	.8	0.	.1	.2													10	5
36	7	1.0	.1	.1	.1	-5.	-10.	-10.										10	8
36	6	.9	.1	.1	.1	.2	.2	.2	.4	1.3								10	
36	5	.9	.1	.2	.3	.3	.3	.4										8	
36	4	1.1	.2	.2	.3	.3	.4	.4	-10.	-15.								9	
36	3	1.9	.5	.5	.5	.7	.9	.8	-10.	-10.								10	
36	2	2.6	.7	1.3	1.8	1.7	1.7	2.0	4.9	-25.								10	
37	8	.8	.1	0.	0.	0.	0.	.1	-10.	-10.								10	8
37	7	.9	0.	0.	0.	0.	.1	.3	.4	.4								10	
37	6	.9	.1	0.	.2	.2	.5	.5	.6	.7								10	
37	5	.9	.07	.07	.07	.2	.6	.6	.8	.9								10	

TABLE A-1. (Cont.) RAW DATA FROM DENSITOMETER ANALYSIS

		LUMINANCE INCREMENT AREAS (ARBITRARY UNITS)																	
P	F	1	2	3	4	5	6	7	8	9	10	11	12	13	14	15	16	S	T
37	4	1.1	0.	0.	.1	.3	1.0	1.1	1.2	1.4								10	
37	3	1.5	.2	0.	.1	.4	1.7	2.2	2.4	2.2								10	
39	→					.2	.6	.1	-25.	-20.								9	7
39	3				.1	.3	.6	.9	2.1	-25.								9	
40	9	.7	0.	0.	.2	-25.													5
40	7	.8	0.	.1	.3	.5	-5.											9	6
40	6	.8	0.	0.	0.	.3	.6	-20.										9	7
40	5	.9	0.	0.	0.	.2	.7	.9	.8									10	
40	4	1.1	.2	.2	.6	1.0	1.5	1.3	.9									10	
40	3	.8	0.	0.	.8	1.8	2.2	1.3	2.3									10	
41	7	1.1	.3	.3	.3	.3	.3	.4										8	
41	6	1.0	.1	.1	.3	.2	.2	.3	.5									9	
41	5	1.0	.3	.3	.4	.3	.4	.6	1.1									10	
41	4	.8	.1	.3	.4	.5	.5	.8										10	
41	3	.7	.4	.3	.3	.3	.3	.4	.7									10	
41	2	1.1	.5	.5	.8	.5	.5	1.4	1.4									10	
42	10						.1	.4	-20.									9	8
42	9	.1	.2	.2	.3	.3	.3	.5										9	8
42	8	.1	.1	.1	.2	.2	.3	.4	.7									10	10
42	7	1.0	.1	.1	.2	.3	.4	.4	.6									10	
42	6	1.2	.3	.4	.6	.6	.6	.6										10	
42	5	1.2	.3	.4	.7	.6	.7	.8	1.0									11	
42	4	1.2	.2	.1	.6	1.0	1.2	1.0	1.6	1.4								11	
42	3	1.4	.2	.6	.6	1.7	2.5	2.1	3.3									10	
43	8				.1	.1	.1	.2	.2	.3	.5	-10.	-15.	-10.	-5.			12	
43	6				.2	.1	.2	.2	.3	.4	-5.	-10.	-10.	-20.				11	
44	7												.1	0.	.2			15	
44	6												.2	.1	.2			15	
44	5											.4	.3	.2	.8			15	
44	4											.7	.5	.5	1.3			16	
44	3										.9	1.0	1.0	.7	1.1			16	
45	9										.4	.9	.6	.4	.5			15	
45	8												.2	.3	.5			16	
45	7										.1	.3	.6	.6	2.2			15	
45	6											.5	1.8	.7	.8			15	
45	5										.8	1.5	1.7	.8	1.2			16	
45	4										.1	1.5	1.5	1.1	1.8			16	

Appendix B
DATA SET FOR MODEL REGISTRATION

This appendix presents the merged data set upon which model registration was effected. In addition to integers useful for identification, the list includes all geometric and luminance values individually required of both the diffuse sphere model and the atmospherics. The contrast values were not employed in the registration but are included here since they have general interest.

TABLE B-1. DATA ARRAY FOR MODEL REGISTRATION

PASS NUMBER	FRAME NUMBER	RADAR DATUM NUMBER	SLANT RANGE (meters)	AIRCRAFT ELEVATION ANGLE (degrees)	SOLAR ELEVATION ANGLE (degrees)	PHASE ANGLE (degrees)	SKY LUMINANCE (ft-L)	MEAN AIRCRAFT LUMINANCE (ft-L)	AIRCRAFT APPARENT CONTRAST
1	9	154	1663.	4.	25.	60.	2550.	2115.	-0.17
1	7	155	1420.	5.	25.	60.	2550.	1793.	-0.30
1	6	156	1176.	6.	25.	59.	2550.	1632.	-0.36
1	5	157	941.	8.	25.	53.	2550.	1817.	-0.29
1	4	158	706.	10.	25.	56.	2550.	1644.	-0.36
1	3	159	481.	16.	25.	55.	2190.	1598.	-0.27
1	2	160	288.	27.	25.	55.	2190.	1556.	-0.29
2	5	265	1363.	5.	26.	52.	2980.	2519.	-0.15
2	4	266	1162.	5.	26.	48.	2980.	2550.	-0.14
2	3	267	994.	6.	26.	42.	2980.	2522.	-0.15
2	1	269	770.	8.	26.	34.	3730.	2491.	-0.33
3	6	402	1272.	6.	26.	125.	3730.	2748.	-0.26
3	5	403	1025.	7.	26.	124.	2980.	2673.	-0.10
3	4	404	782.	9.	26.	123.	2980.	2315.	-0.22
3	3	405	541.	14.	26.	121.	2980.	2661.	-0.11
3	2	406	319.	24.	26.	114.	2550.	3559.	0.40
4	7	484	1433.	5.	27.	80.	2550.	1916.	-0.25
4	6	485	1200.	6.	27.	84.	2550.	1873.	-0.27
4	5	486	976.	7.	27.	89.	2980.	1779.	-0.40
4	4	487	767.	10.	27.	98.	2980.	1845.	-0.38
4	3	488	591.	13.	27.	112.	2980.	1606.	-0.46
4	2	489	485.	16.	27.	136.	2980.	1449.	-0.51
5	7	565	1620.	3.	27.	49.	2550.	2140.	-0.16
5	6	566	1422.	4.	27.	45.	2550.	2190.	-0.14
5	5	567	1235.	5.	27.	41.	2550.	2079.	-0.18
5	4	568	1079.	5.	27.	37.	2550.	2127.	-0.16
5	3	569	963.	6.	27.	34.	2550.	2019.	-0.21
5	2	570	901.	7.	27.	36.	2550.	2152.	-0.16
5	1	571	905.	7.	27.	43.	2980.	1895.	-0.36
6	6	617	1605.	4.	28.	127.	3730.	2547.	-0.30
6	5	618	1354.	5.	28.	127.	3730.	2339.	-0.27
6	4	619	1105.	6.	28.	127.	3730.	2607.	-0.30
6	3	620	857.	8.	28.	126.	2980.	2425.	-0.19
6	2	621	611.	11.	28.	126.	2550.	2332.	-0.09
8	3	824	1214.	4.	29.	37.	2980.	2465.	-0.17
8	1	826	1092.	4.	29.	33.	2980.	2266.	-0.24
9	8	900	2023.	3.	29.	64.	2550.	1977.	-0.22
9	7	901	1810.	4.	29.	58.	2550.	1719.	-0.33
9	6	902	1608.	4.	29.	72.	2550.	1954.	-0.23
9	5	903	1425.	5.	29.	79.	2550.	1903.	-0.25
9	4	904	1266.	6.	29.	86.	2980.	2056.	-0.31
9	3	905	1142.	6.	29.	96.	2980.	1776.	-0.40
9	1	907	1057.	7.	29.	119.	2980.	1942.	-0.35
11	4	1094	961.	7.	30.	50.	2980.	2019.	-0.32
11	3	1095	833.	8.	30.	43.	2980.	1981.	-0.34
11	2	1096	771.	9.	30.	39.	2980.	1998.	-0.33
11	1	1097	785.	8.	30.	41.	2980.	1986.	-0.33
15	6	1492	1395.	6.	34.	84.	2550.	1538.	-0.40
15	5	1493	1205.	7.	34.	89.	2550.	1449.	-0.43
15	4	1494	1035.	9.	34.	97.	2980.	1501.	-0.50
18	9	1822	1340.	6.	35.	68.	2550.	1861.	-0.27
18	8	1823	1141.	7.	35.	73.	2550.	1845.	-0.28
18	7	1824	957.	8.	35.	79.	2550.	1960.	-0.23
18	6	1825	795.	10.	35.	89.	1890.	1263.	-0.33
18	5	1826	672.	12.	35.	102.	2190.	1511.	-0.31
22	9	2360	2231.	2.	38.	41.	2980.	2430.	-0.18
22	8	2361	2001.	3.	38.	41.	2980.	2430.	-0.18
22	7	2362	1781.	3.	38.	43.	2980.	2370.	-0.20

TABLE B-1. (Cont.) DATA ARRAY FOR MODEL REGISTRATION

PASS NUMBER	FRAME NUMBER	RADAR DATUM NUMBER	SLANT RANGE (meters)	AIRCRAFT ELEVATION ANGLE (degrees)	SOLAR ELEVATION ANGLE (degrees)	PHASE ANGLE (degrees)	SKY LUMINANCE (ft-L)	MEAN AIRCRAFT LUMINANCE (ft-L)	AIRCRAFT APPARENT CONTRAST
22	6	2363	1567.	3.	38.	44.	2980.	2370.	-0.20
22	5	2364	1369.	4.	38.	47.	2980.	2314.	-0.22
22	3	2366	1053.	5.	38.	58.	2980.	2248.	-0.25
23	5	2467	1207.	6.	38.	82.	3730.	3027.	-0.19
23	4	2468	1015.	7.	38.	77.	2550.	2806.	0.10
23	3	2469	853.	9.	38.	69.	2550.	2171.	-0.15
27	12	2827	2797.	3.	40.	72.	2550.	1627.	-0.36
27	11	2828	2559.	3.	40.	74.	2550.	1669.	-0.35
27	10	2829	2323.	3.	40.	75.	2550.	1536.	-0.40
27	9	2830	2089.	3.	40.	77.	2550.	1593.	-0.38
27	8	2831	1862.	4.	40.	80.	2550.	1555.	-0.39
27	7	2832	1640.	4.	40.	83.	2550.	1500.	-0.41
27	6	2833	1429.	5.	40.	88.	2550.	1469.	-0.42
27	5	2834	1235.	6.	40.	94.	2190.	1362.	-0.38
27	4	2835	1066.	7.	40.	101.	2550.	1640.	-0.36
27	2	2837	960.	9.	40.	124.	3730.	1703.	-0.54
28	8	2893	2156.	2.	40.	135.	3730.	2819.	-0.24
28	7	2894	1978.	3.	40.	132.	3730.	2686.	-0.28
28	6	2895	1819.	3.	40.	129.	3730.	2611.	-0.30
28	5	2896	1683.	4.	40.	125.	3730.	2504.	-0.33
28	4	2897	1578.	4.	40.	119.	2980.	2154.	-0.28
28	3	2898	1507.	5.	40.	113.	2980.	2126.	-0.29
28	2	2899	1479.	5.	40.	106.	2980.	2133.	-0.28
28	1	2900	1495.	5.	40.	99.	2980.	1865.	-0.37
28	-2	2902	1651.	5.	40.	85.	2550.	1643.	-0.36
28	-3	2903	1780.	5.	40.	79.	2550.	1980.	-0.22
28	-4	2904	1934.	4.	40.	74.	2550.	1631.	-0.36
30	14	3093	3229.	1.	40.	42.	3730.	2406.	-0.35
30	13	3094	2982.	2.	40.	42.	3730.	2320.	-0.38
30	12	3095	2737.	2.	40.	42.	3730.	2370.	-0.36
30	11	3096	2493.	2.	40.	43.	3730.	2310.	-0.38
30	10	3097	2246.	2.	40.	43.	3730.	2194.	-0.41
30	9	3098	2012.	3.	40.	43.	3730.	2131.	-0.43
30	8	3099	1781.	3.	40.	44.	3730.	1999.	-0.46
30	7	3100	1564.	3.	40.	46.	2980.	1949.	-0.35
32	5	3328	1308.	4.	41.	44.	2980.	1796.	-0.40
32	4	3329	1134.	4.	41.	46.	2550.	1995.	-0.22
33	9	3403	2321.	3.	41.	122.	2980.	1893.	-0.36
33	8	3404	2086.	3.	41.	124.	2980.	1930.	-0.35
33	7	3405	1858.	4.	41.	127.	2980.	1733.	-0.42
33	6	3406	1642.	4.	41.	131.	2980.	1835.	-0.38
33	5	3407	1443.	5.	41.	135.	3730.	2144.	-0.43
33	4	3408	1271.	5.	41.	140.	3730.	2060.	-0.45
33	3	3409	1131.	6.	41.	144.	3730.	2097.	-0.44
33	1	3411	1017.	7.	41.	142.	3730.	2201.	-0.41
35	3	3619	558.	5.	19.	49.	2190.	1562.	-0.29
35	2	3620	417.	7.	19.	31.	1890.	1723.	-0.09
44	7	4481	1582.	6.	15.	169.	4500.	3337.	-0.26
44	6	4482	1333.	7.	15.	170.	4500.	3108.	-0.31
44	5	4483	1085.	9.	15.	171.	4500.	3071.	-0.32
44	4	4484	843.	12.	15.	171.	5260.	3049.	-0.42
44	3	4485	603.	18.	15.	170.	5260.	2697.	-0.49
45	9	4568	1900.	4.	14.	169.	4500.	2612.	-0.42
45	8	4569	1688.	5.	14.	168.	5260.	3269.	-0.38
45	7	4570	1484.	6.	14.	166.	4500.	3255.	-0.28
45	6	4571	1280.	7.	14.	164.	4500.	2330.	-0.37
45	5	4572	1092.	9.	14.	159.	5260.	2665.	-0.49
45	4	4573	916.	11.	14.	152.	5260.	2892.	-0.45

Appendix C
KOSCHMIEDER'S EQUATION

Koschmieder"s equation is derived here from a more general form of the transport equation. The reason for including a derivation is that the assumptions necessary for validity and the expression for "equilibrium luminance" for the atmosphere both occur naturally.

Ignoring polarization, the propagation of brightness (luminance) in an absorbing and incoherent scattering atmosphere is in accord with the well-known expression (e.g., Middleton[8]):

$$B = \left(B_o + \int_0^x S(x') \, e^{\tau(x')} \, dx' \right) e^{-\tau(x)} \qquad \text{(C-1)}$$

Here, B_o is inherent brightness at $x = 0$, and B is apparent brightness at a distance X. $S(x)$ is a veiling brightness source term given by:

$$S = \oint k \, B_S \, d\Omega \qquad \text{(C-2)}$$

where B_S is the surround brightness for a given point on the path, and k is the volume scattering coefficient. The parameter τ (optical thickness) is defined as follows:

$$\tau(x) \equiv \int_0^x \beta(x') \, dx' \qquad \text{(C-3)}$$

where β is the attenuation coefficient. Finally, one further term, the scattering phase function, $\hat{k}$, is defined:

$$\hat{k} \equiv k/\beta \qquad \text{(C-4)}$$

8. W.E.K. Middleton, "Vision Through the Atmosphere," University of Toronto Press, 1968.

Since both the volume scattering coefficient and the attenuation coefficient are directly proportional to atmospheric concentration, $\hat{k}$ depends on the physical nature of the scattering medium, but not on concentration.

The approximation that leads to Koschmieder's equation is to take both $\hat{k}$ and B_s as independent of path position. With manipulation, Equation (C-1) becomes:

$$B = B_0 e^{-\tau(x)} + \left(\oint \hat{k} B_s \, d\Omega\right)\left(1 - e^{-\tau(x)}\right) \tag{C-5}$$

For an infinitely thick path ($\tau \to \infty$), the "equilibrium brightness", B_∞, can be defined,

$$B_\infty = \oint \hat{k} B_s \, d\Omega \tag{C-6}$$

and, therefore:

$$B = B_0 e^{-\tau(x)} + B_\infty \left(1 - e^{-\tau(x)}\right), \tag{C-7}$$

a popular form of Koschmieder's equation.